THESIS

MIDLATITUDE PREDICTION SKILL FOLLOWING QBO-MJO ACTIVITY ON SUBSEASONAL TO SEASONAL TIMESCALES

Submitted by

Kirsten J. Mayer

Department of Atmospheric Science

In partial fulfillment of the requirements

For the Degree of Master of Science

Colorado State University

Fort Collins, Colorado

Fall 2019

Master's Committee:

Advisor: Elizabeth A. Barnes

Eric Maloney
Chuck Anderson

ABSTRACT

MIDLATITUDE PREDICTION SKILL FOLLOWING QBO-MJO ACTIVITY ON SUBSEASONAL TO SEASONAL TIMESCALES

The Madden-Julian Oscillation (MJO) is known to force extratropical weather days-to-weeks following an MJO event through excitation of Rossby waves, also known as tropical-extratropical teleconnections. Prior research has demonstrated that this tropically forced midlatitude response can lead to increased prediction skill on subseasonal to seasonal (S2S) timescales. Furthermore, the Quasi-Biennial Oscillation (QBO) has been shown to possibly alter these teleconnections through modulation of the MJO itself and the atmospheric basic state upon which the Rossby waves propagate. This implies that the MJO-QBO relationship may affect midlatitude circulation prediction skill on S2S timescales. In this study, we quantify midlatitude circulation sensitivity and prediction skill following active MJOs and QBOs across the Northern Hemisphere on S2S timescales through an examination of the 500 hPa geopotential height field. First, a comparison of the spatial distribution of Northern Hemisphere sensitivity to the MJO during different QBO phases is performed for ERA-Interim reanalysis as well as ECMWF and NCEP hindcasts. Secondly, differences in prediction skill in ECMWF and NCEP hindcasts are quantified following MJO-QBO activity. We find that regions across the Pacific, North America and the Atlantic exhibit increased prediction skill following MJO-QBO activity, but these regions are not always collocated with the locations most sensitive to the MJO under a particular QBO state. Both hindcast systems demonstrate enhanced prediction skill 7-14 days following active MJO events during strong QBO periods compared to MJO events during neutral QBO periods.

ACKNOWLEDGMENTS

I would like to thank Dr. Elizabeth Barnes for her mentorship and guidance through the completion of this thesis as well as Dr. Eric Maloney and Dr. Chuck Anderson, for their roles on my graduate committee. This research was supported by the NOAA MAPP S2S Prediciton Task force.

TABLE OF CONTENTS

LIST OF FIGURES

CHAPTER 1

INTRODUCTION

Previous research has focused on the impact of the Madden-Julian Oscillation (MJO) on the extratropical circulation in order to extend midlatitude prediction skill (e.g. Henderson et al. 2016; Baggett et al. 2017; Tseng et al. 2018; Zheng et al. 2018). The MJO is a 20-90 day tropical intraseasonal convective oscillation (Madden and Julian 1971, 1972, 1994), and through its convective heating, initiates an extratropical response through the excitation of Rossby waves. These waves modulate the mid-latitude circulation days to weeks following MJO activity and have been shown to provide coherent and consistent modulation of midlatitude circulation into subseasonal-to-seasonal (2-5 Weeks; S2S hereafter) timescales (e.g. Hoskins and Karoly 1981; Sardeshmukh and Hoskins 1988; Henderson et al. 2016; Tseng et al. 2018).

More recent research has demonstrated a dependence of the MJO on a stratospheric phenomenon known as the Quasi-biennial Oscillation (QBO). The QBO is an approximately 28 month, downward propagating zonal mean, zonal wind oscillation in the tropical stratosphere and has many subsequent impacts such as modulation of the upper tropical troposphere (e.g. Collimore et al. 2003; Garfinkel and Hartmann 2011b; Son et al. 2017), the subtropical jet (e.g. Simpson et al. 2009; Garfinkel and Hartmann 2011a) and the stratospheric polar vortex (e.g. Holton and Tan 1980; Garfinkel et al. 2018). The QBO is typically divided into two phases, easterly and westerly (EQBO and WQBO, respectively), determined by the direction of the anomalous zonal wind in the lower tropical stratosphere (Baldwin et al. 2001). Recent work has shown that the MJO convective envelope tends to be stronger and have slower eastward propagation and longer path lengths during EQBO compared to WQBO (Son et al. 2017; Nishimoto and Yoden 2017; Densmore et al. 2019; Zhang and Zhang 2018). Son et al. (2017) hypothesize that this slower MJO propagation during EQBO is a consequence of strengthened MJO convection, as stronger MJO events tend to propagate more slowly across the Maritime Continent. However, Zhang and Zhang (2018) argue that stronger MJO wintertime events during EQBO are a consequence of a greater number of MJO days instead of larger amplitudes of individual MJO events. While there are still uncertainties regarding the exact impacts of the QBO on the MJO, these studies demonstrate the importance of considering the QBO in MJO research.

Much of the recent MJO-QBO research has focused on the direct impacts of the QBO on the tropical tropopause, and thus, MJO activity, while only a handful of studies have examined how the QBO subsequently impacts MJO teleconnections (Baggett et al. 2017; Mundhenk et al. 2018; Wang et al. 2018). Baggett et al. (2017) and Mundhenk et al. (2018) emphasize the impact of the QBO on MJO teleconnections through its modulation of MJO-induced Rossby waves, and consequently, changes in the steering and frequency of atmospheric rivers. Wang et al. (2018) found that when accounting for the phase of the QBO, the amplitude of the North Pacific storm track shift in response to MJO activity is greater during EQBO compared to WQBO, which they hypothesize to be from increased MJO strength during EQBO.

A MJO-QBO relationship has also been found in dynamical models. For example, Abhik and Hendon (2019) recently demonstrated that hindcast simulations, initialized with observations during active MJOs, capture the increase in MJO amplitude and maintenance during EQBO events after about 5 days. In addition, this strengthened MJO amplitude during EQBO has been shown to translate to increased MJO prediction skill (Marshall et al. 2017; Lim et al. 2019), suggesting that the prediction skill of the subsequent midlatitude teleconnections may also increase following the MJO under EQBO conditions. Baggett et al. (2017) further show that S2S prediction skill of atmospheric rivers is increased within ECMWF hindcasts over North America out to 3 weeks following MJO activity. This highlights the potential for an MJO-QBO relationship to modulate midlatitude prediction skill on S2S timescales.

Since hindcast models capture the increase in MJO amplitude during EQBO as well as exhibit enhanced prediction skill of the MJO in Weeks 1-3 under strong QBOs, this raises the question as to whether the MJO-QBO relationship also translates to enhanced prediction skill of MJO teleconnections under specific QBO phases. This paper explores this question through an analysis of the influence of the QBO on midlatitude prediction skill following active MJOs on S2S timescales within the ECMWF and NCEP hindcasts.

CHAPTER 2

DATA AND METHODS

2.1 DATA

We utilize daily mean 500-hPa geopotential height (z500; years 1979-2017) from the European Centre for Medium-Range Weather Forecasts Interim reanalysis (ERA-I; Dee et al. 2011) as well as the ECMWF and NCEP hindcasts obtained from the S2S database (Vitart 2017) established by the World Weather Research Program/World Climate Research Program (WWRP/WCRP). The ECMWF hindcasts are initialized 4 times a week (years 1995-2016). The NCEP hindcasts are initialized daily (years 1999-2010). In the following analysis, the control run for both models are used. We use the control run rather than the ensemble mean for a better comparison between the models, since ECMWF has 11 ensembles while NCEP has 4. Since we use the control run, these results should not be used as an analysis of the efficacy of the ECMWF and NCEP hindcasts, but rather, an analysis and comparison of prediction skill within and between both models.

We focus on December, January and February (DJF) since MJO teleconnections are strongest during boreal winter (e.g. Madden 1986), and the relationship between the MJO and QBO is strongest during these months as well (e.g. Yoo and Son 2016; Son et al. 2017). The annual cycle is removed from the ERA-I reanalysis by subtracting the daily climatology of z500 across 1979-2017 from the z500 field. For the hindcast models, a daily, lead-dependent climatology is subtracted from each models' z500 field. To do this, we calculate the daily climatology for each lead time independently. Since the ECMWF model is not initialized daily, two (forward and backward moving) 31-day running means are applied to the climatology at all lead times to reduce noise, following Sun et al. (2018). These smoothed lead-dependent daily climatologies are then subtracted from the z500 field of the corresponding model to remove the annual cycle.

There is presently no definitive understanding of the impact of the El Nino Southern Oscillation (ENSO) on the QBO-MJO relationship. Some earlier research indicates that ENSO has a limited impact on the QBO-MJO interaction (e.g. Yoo and Son 2016; Nishimoto and Yoden 2017); however, recent work on QBO-MJO teleconnections has shown a possible dependency of results on ENSO (Son et al. 2017; Wang et al. 2018; Sun et al. 2019). Thus, in an attempt to ensure our results are not somehow biased by ENSO, we use the Nino3.4 Index (climatedataguide.ucar.edu/climate-data) to remove strong ENSO winter seasons from our analysis. Specifically, when the amplitude of the NINO3.4 index for a

month within DJF is greater than 1°C (signifying El Nino) or less than -1°C (signifying La Nina), that DJF season is excluded from the analysis. With that said, we have repeated our analysis with ENSO seasons included and find our conclusions remain the same (see Appendix Figures A7-A10).

2.2 MJO AND QBO INDICES

The real-time multivariate MJO (RMM) index is used to define the amplitude and phase of the MJO in the ERA-I reanalysis (Wheeler and Hendon 2004). This index uses empirical orthogonal function (EOF) analysis applied to anomalous outgoing longwave radiation (OLR) and 200- and 850-hPa zonal wind, near-equatorially averaged (15°S to 15°N), to determine the first two principal components (RMM1 and RMM2). A day is considered to have an active MJO when the RMM amplitude for that day (defined as $\sqrt{(RMM1^2 + RMM2^2)}$) is greater than 1.0. The MJO phase is then defined as $tan^{-1}(RMM2/RMM1)$ and largely corresponds to the longitudinal location of the convective envelope. Active MJO dates within ERA-I that correspond to initialization dates in ECMWF and NCEP are determined from this index. The RMM index is not separately calculated for each hindcast model because we do not aim to quantify the ability of the models to forecast the MJO directly (e.g. Vitart 2017). Rather, we use the index calculated from reanalysis to see how the hindcast models initialized on observed active MJO days ultimately forecast MJO teleconnections.

Identical to the definition of (Yoo and Son 2016), the QBO index is calculated within ERA-I using monthly standardized zonal wind at 50-hPa, area-averaged between 10°S to 10°N. Westerly QBO (WQBO) and Easterly QBO (EQBO) events are defined as when the standardized value is greater than 0.5σ or less than -0.5σ, respectively. Absolute values less than 0.5σ are considered neutral QBO (NQBO) events.

2.3 METHODS

Quantification of each models' ability to represent MJO teleconnections under different QBO phases is conducted using the Sensitivity to the Remote Influence of Periodic Events (STRIPES) index (Jenney et al. 2019). STRIPES is an index recently developed to determine regions of extratropical sensitivity to remote periodic events such as the MJO. As used here, the STRIPES index quantifies the strength and consistency of MJO teleconnections in z500 through average phase and 0-21 day lead information at individual grid points for a variety of observed phase speeds (5-8 days/phase; Wheeler and Hendon 2004). Specifically, a composite of average z500 anomalies for each MJO phase and lead is created for each grid point in the Northern Hemisphere. If a region is sensitive to the MJO, we expect alternating

z500 anomaly stripes sloped at the phase speed of the MJO in the phase versus lead diagram (as seen in Appendix Figure A1 for example). Regions not sensitive to the MJO will appear noisy with smaller amplitudes and less coherent stripes. Averages along the slopes corresponding to the MJO phase speed are calculated, and if there are alternating stripes (i.e. sensitivity to the MJO), the resultant vector will look like a sine wave, for which the amplitude can be calculated. The resulting amplitude of this oscillatory vector is the STRIPES index (Jenney et al. 2019). Therefore, the more sensitive the region is to MJO teleconnections, the larger the STRIPES index.

Since our application focuses on extratropical sensitivity in z500, we do not standardize our data for STRIPES as in Jenney et al. (2019). Standardization may mute the extratropical signal due to the greater variability of z500 in the midlatitudes, which is of main interest here. For equal comparison of STRIPES between the models and reanalysis, we calculate STRIPES for ERA-I only with dates that overlap with the hindcasts. Thus, the ERA-I STRIPES figures differ for ECMWF versus NCEP dates.

STRIPES values that are statistically larger than expected by chance are determined using the bootstrapping method. The number of random days grabbed corresponds to the observed number of days for the QBO-MJO event of interest. In order to retain autocorrelation within MJO events, we keep the day-of-year (doy) and phase distribution information for each MJO event and randomly sample years (with replacement). Since the ECMWF hindcast data is not initialized on the same day each year, if the doy needed is not available for a particular year, we instead use the date of initialization closest to this doy. From this sample, we calculate STRIPES. This is repeated 250 times for each latitude and longitude. We only repeat this calculation 250 times due to computational limits. Any STRIPES value greater than the 90^{th} percentile of these bootstrapped values are deemed significant. Since autocorrelation is retained, this statistical analysis is more difficult to pass, and thus, the 90^{th} percentile was used instead of the 95^{th} percentile. Note, that when all MJO days are included (see Appendix Figure A3), the statistical analysis shows significance in regions of large STRIPES values. However, when the data is subdivided by QBO phase, we begin to see the effects of sample size on the uncertainty, leading to fewer points of significance. This bootstrapping analysis is only conducted on ERA-I, as these are the 'observed' sensitivities and thus, the regions of interest.

To quantify midlatitude prediction skill, a daily area-weighted Pearson correlation is conducted between hindcast and ERA-I anomalous z500 (anomaly correlation coefficient; ACC). The data is separated into NQBO-, EQBO- and WQBO-(inactive)MJO events in each hindcast dataset and the corresponding reanalysis data is obtained from ERA-I. The ACC between a given model day and the same

day in ERA-I is calculated within a centered 60° longitude wide box extending from 30-60° N. Our conclusions are not affected by the latitudinal extent of the box when it is varied by +/- 10-30 °N. This calculation is repeated for every initialization and subsequent lead time as well as every 5° longitude beginning at 0°E. ACCs are grouped and averaged by QBO phase to obtain average ACCs across the Northern Hemisphere at every lead for each QBO phase (see Appendix Figure A2 for an example). Differences between EQBO- or WQBO-MJO ACCs and NQBO-MJO ACCs capture the additional midlatitude prediction skill following active MJOs during E/WQBO compared to neutral QBO. Differences between E/W-MJO ACCs and E/WQBO-inactive MJO ACCs capture the additional midlatitude prediction skill following active MJOs during a particular strong phase of the QBO.

Statistically significant differences in ACCs across lead and longitude are also computed with the bootstrapping method. Specifically, all model data within DJF is shuffled and random dates are grabbed. The number of random dates corresponds to the number of observed dates for the particular QBO phase and MJO activity being tested. The corresponding random dates are then found in ERA-I. The spatial correlations between the model and the observations are calculated and then averaged to get an average ACC. This is repeated for each QBO-MJO combination, and the differences between their ACCs is calculated. The above analysis is repeated 10,000 times for each longitude and lead time. Differences greater than the 97.5^{th} percentile of the 10,000 bootstrapped differences are considered significantly greater from that expected by chance. In this bootstrapping analysis, we were able to repeat the calculations 10,000 times (instead of 250) because the calculation was less computationally expensive.

CHAPTER 3

RESULTS: EXTRATROPICAL SENSITIVITY

The left column of Figure 3.1 shows the STRIPES analysis of ERA-I for days within the ECMWF hindcasts, split by QBO phase. Darker shading indicates regions of greater sensitivity to the MJO for each QBO state. Regions along the North Pacific and Atlantic storm tracks as well as over North America are sensitive to the MJO for all phases of the QBO (Figure 3.1a,c,e). This is consistent with previous research as these regions have been shown to be sensitive to MJO excited Rossby waves through, for example, their modulation of the North Atlantic Oscillation (Cassou 2008), the Pacific North American Oscillation (Mori and Watanabe 2008) and Northern Hemisphere wintertime blocking (Henderson et al. 2016).

The right column of Figure 3.1 shows the STRIPES analysis of the ECMWF hindcasts for the same dates. ECMWF largely captures the spatial patterns and locations sensitive to the MJO under different QBO phases (spatial correlation with ERA-I: $r_{NQBO-MJO} = 0.93$, $r_{EQBO-MJO} = 0.97$, and $r_{WQBO-MJO} = 0.94$), but overall the model has smaller STRIPES values than ERA-I. This is likely a result of model forecast degradation at later lead times since the calculation of STRIPES utilizes z500 forecasts out to 21 days lead time.

An examination of the NCEP hindcasts shows that it also generally captures regions sensitive to the MJO under varying phases of the QBO (Figure 3.2b,d,f; spatial correlation with ERA-I: $r_{NQBO-MJO} = 0.93$, $r_{EQBO-MJO} = 0.95$, and $r_{WQBO-MJO} = 0.95$) and is also weaker than the corresponding ERA-I analysis (Figure 3.2a,c,e). The ERA-I STRIPES analysis for NCEP hindcasts largely has the same features as the ERA-I analysis for ECMWF hindcasts, but with larger values due to differences in sample size and dates of initialization between NCEP and ECMWF. From this STRIPES comparison (Figures 3.1 and 3.2), we conclude that the ECMWF and NCEP hindcast models generally capture Northern Hemisphere regions sensitive to the MJO.

Recent research has shown that during EQBO, the MJO amplitude is larger and the convective envelope propagates slower compared to MJO activity during WQBO (Son et al. 2017; Nishimoto and Yoden 2017; Zhang and Zhang 2018). If direct impacts to the MJO (e.g. through changes in tropical static stability) lead to changes in MJO teleconnection sensitivity across the Northern Hemisphere, we might expect EQBO-MJO events to have larger midlatitude sensitivity to the MJO compared to WQBO-MJO. Based on our STRIPES analysis, we find that Northern Hemisphere sensitivity to the MJO is significantly reduced during EQBO-MJO events compared to WQBO-MJO events (compare Figure 3.1c,e and

Figure 3.2c,e; significance not shown). We explored this further and found that this difference can be explained by the tendency for WQBO to have larger magnitude z500 anomalies compared to EQBO, not more distinct stripes. In other words, when the amplitude differences between the z500 anomalies are accounted for through normalization, the difference in Northern Hemispheric sensitivity to the MJO between QBO phases is greatly reduced (Figure 3.3). The data is normalized by dividing by the average absolute value of the Phase vs Lead diagram for each latitude-longitude point prior to computing the STRIPES index. By doing so, we are able to reduce the impact of the anomaly magnitude on the STRIPES index, and thus, the index mainly provides information on the "stripey-ness".

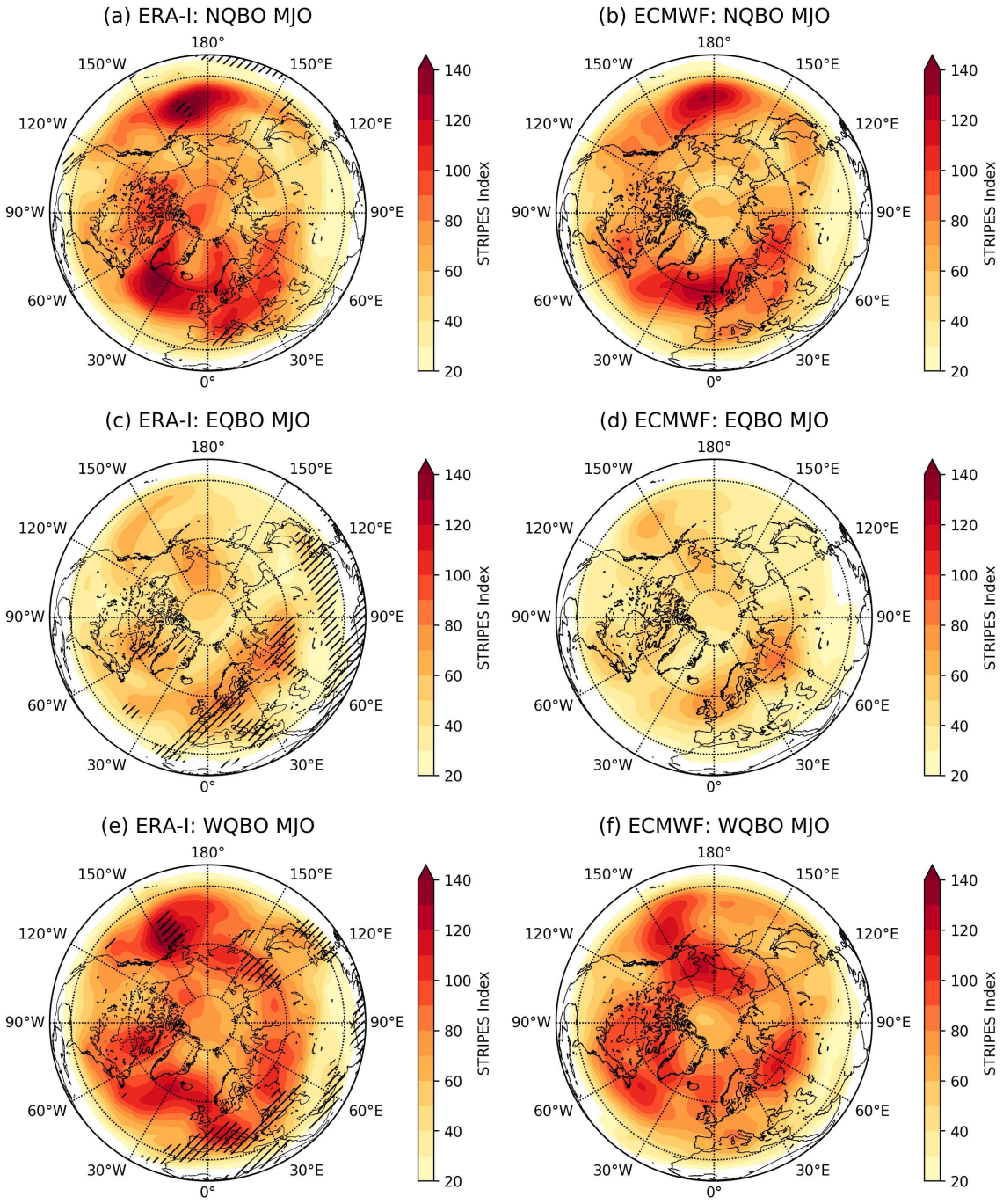

FIG. 3.1. STRIPES values for (left) ERA-Interim and (right) ECMWF for all (top) NQBO-MJO, (middle) EQBO-MJO and (bottom) WQBO-MJO events. Black hatches denote STRIPES values that are statistically larger than expected by chance at 90% confidence in ERA-I.

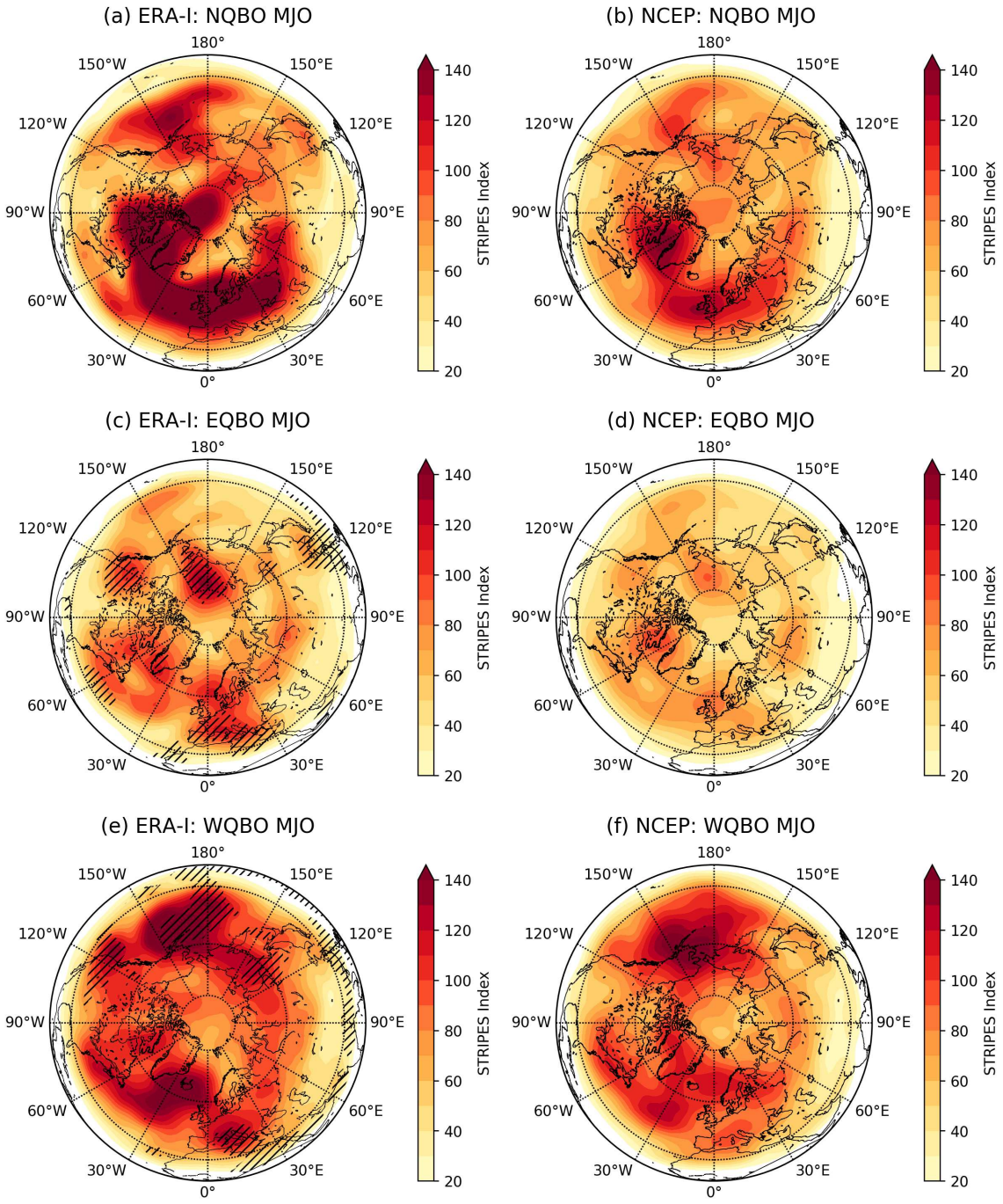

FIG. 3.2. STRIPES values for (left) ERA-Interim and (right) NCEP for all (top) NQBO-MJO, (middle) EQBO-MJO and (bottom) WQBO-MJO events. Black hatches denote STRIPES values that are statistically larger than expected by chance at 90% confidence in ERA-I.

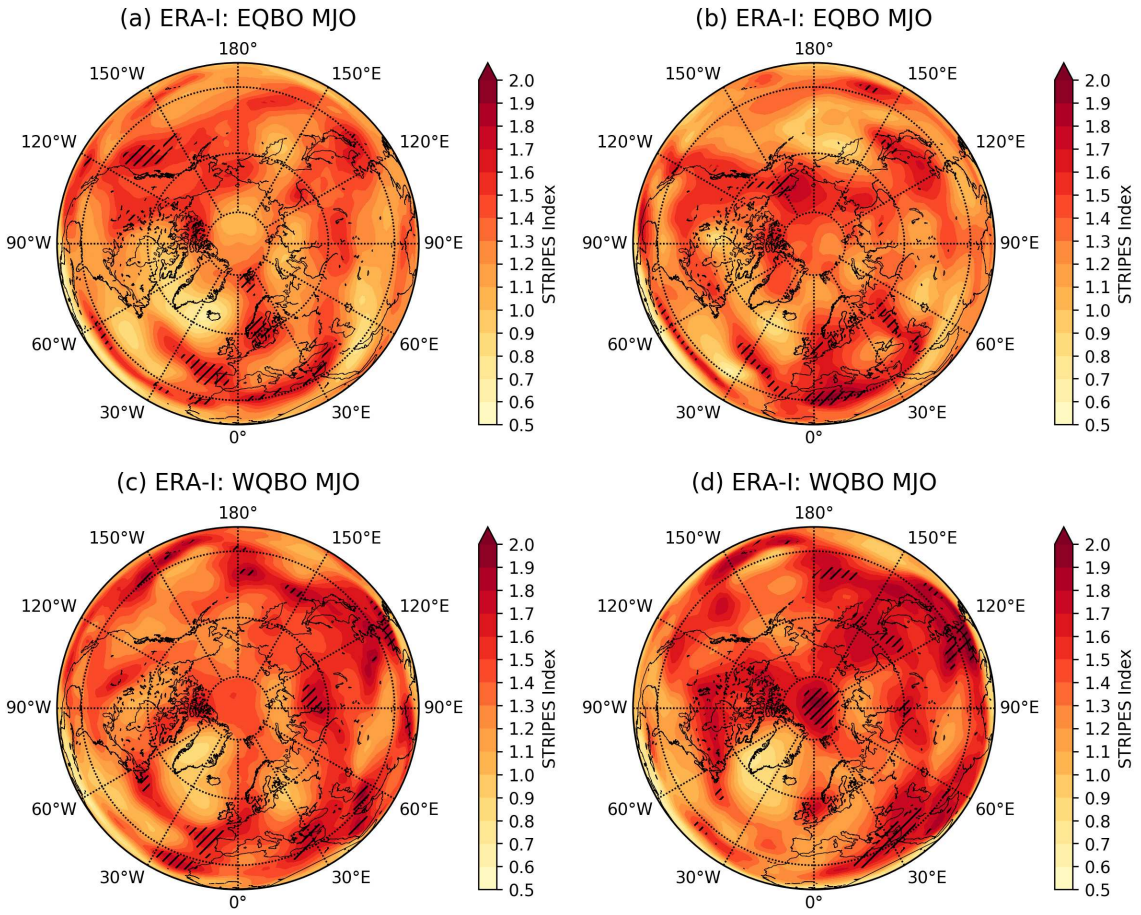

FIG. 3.3. Normalized STRIPES values for (left) ECMWF hindcasts' dates in ERA-I and (right) NCEP hindcasts' dates in ERA-I for (top) EQBO-MJO and (bottom) WQBO-MJO events. Black hatches denote STRIPES values that are statistically larger than expected by chance at 90% confidence in ERA-I. Data is normalized by dividing by the average absolute value of the Phase vs Lead diagram for each latitude-longitude point and then calculating STRIPES on these normalized values.

CHAPTER 4

RESULTS: PREDICTION SKILL

4.1 REGIONAL PREDICTION SKILL

Knowing that the ECMWF and NCEP hindcasts generally capture regional sensitivity to the MJO, we next address whether the QBO impacts midlatitude skill during MJO events and whether regions of increased sensitivity to MJO-QBO activity translate to increased prediction skill. Here, skill is calculated as an anomaly spatial correlation between z500 from the hindcasts and ERA-I (see Chapter 2 Section 3), and we compare this skill over active QBO-MJO combinations to skill during NQBO-MJO and inactive MJO. As mentioned in Chapter 1, EQBO has been found to impact the MJO in ways that may enhance MJO teleconnections (e.g. Son et al. 2017; Nishimoto and Yoden 2017). Since enhanced activity may provide a prominent signal above model noise and uncertainty, and thus, hypothetically lead to enhanced prediction skill, we focus here on only improved prediction skill (see Appendix Figures A4-A5 for regions of decreased prediction skill).

Figure 4.1 shows z500 anomaly prediction skill as a function of lead time for the North Pacific (165°W), North Atlantic (30°W), and Europe regions (0°E). There are multiple ways to think about skill following MJO-QBO activity and therefore we include two types of statistical information. The first type of significance (hollow circles) represents the impact of the phase of strong QBOs on prediction skill compared to NQBO during active MJO. In other words, where there is more skill following E/WQBO-MJO (orange/teal solid) than NQBO-MJO (black solid). The second type of significance (colored dots) represents changes in prediction skill following active MJOs compared to inactive MJOs during a particular QBO phase, or said another way, where E/W/NQBO-MJO (solid) leads to more skill than E/W/NQBO-noMJO (dashed). The presence of both of these forms of significance (colored dots within the hollow circles) represents where there is greater prediction skill following active MJOs compared to inactive MJOs during a particular QBO phase *and* active MJOs during NQBO. When these two significances appear together, we can say that a particular strong QBO increases the impact of the MJO on midlatitude prediction skill.

First we focus on the differences in skill between strong QBO phases and NQBO following active MJOs (hollow circles). For ECMWF, the North Atlantic and Europe (Figure 4.1c,e) have significantly

increased prediction skill into Week 3 following WQBO-MJO (hollow circles on solid teal line) compared to NQBO-MJO. For NCEP, there is significantly increased prediction skill through Week 2 following EQBO-MJO in the North Pacific and WQBO-MJO in the North Atlantic (Figure 4.1b,d).

Focusing next on differences in skill between active and inactive MJOs during strong QBO phases, the MJO leads to enhanced prediction skill compared to inactive MJO in the North Atlantic and Europe during both EQBO and WQBO in ECMWF (Figure 4.1c,e; teal and orange dots), but only in the North Atlantic and during EQBO in NCEP (Figure 4.1d; orange dots). For all of these cases, this increase in prediction skill following the MJO is not present during NQBO, and suggests that the changes to the basic state and/or to the MJO itself during EQBO over the North Atlantic for NCEP and EQBO and WQBO over the North Atlantic and Europe for ECMWF is associated with enhanced midlatitude MJO impact.

The presence of both of these forms of significance (colored dots within the hollow circles) represents where a particular strong QBO increases the impact of the MJO on midlatitude prediction skill. In the three regions depicted in Figure 4.1, the two forms of significance overlap for ECMWF over the North Atlantic and Europe through Week 3 (Figure 4.1c,e; teal dots inside hollow circles), and rarely overlap for NCEP.

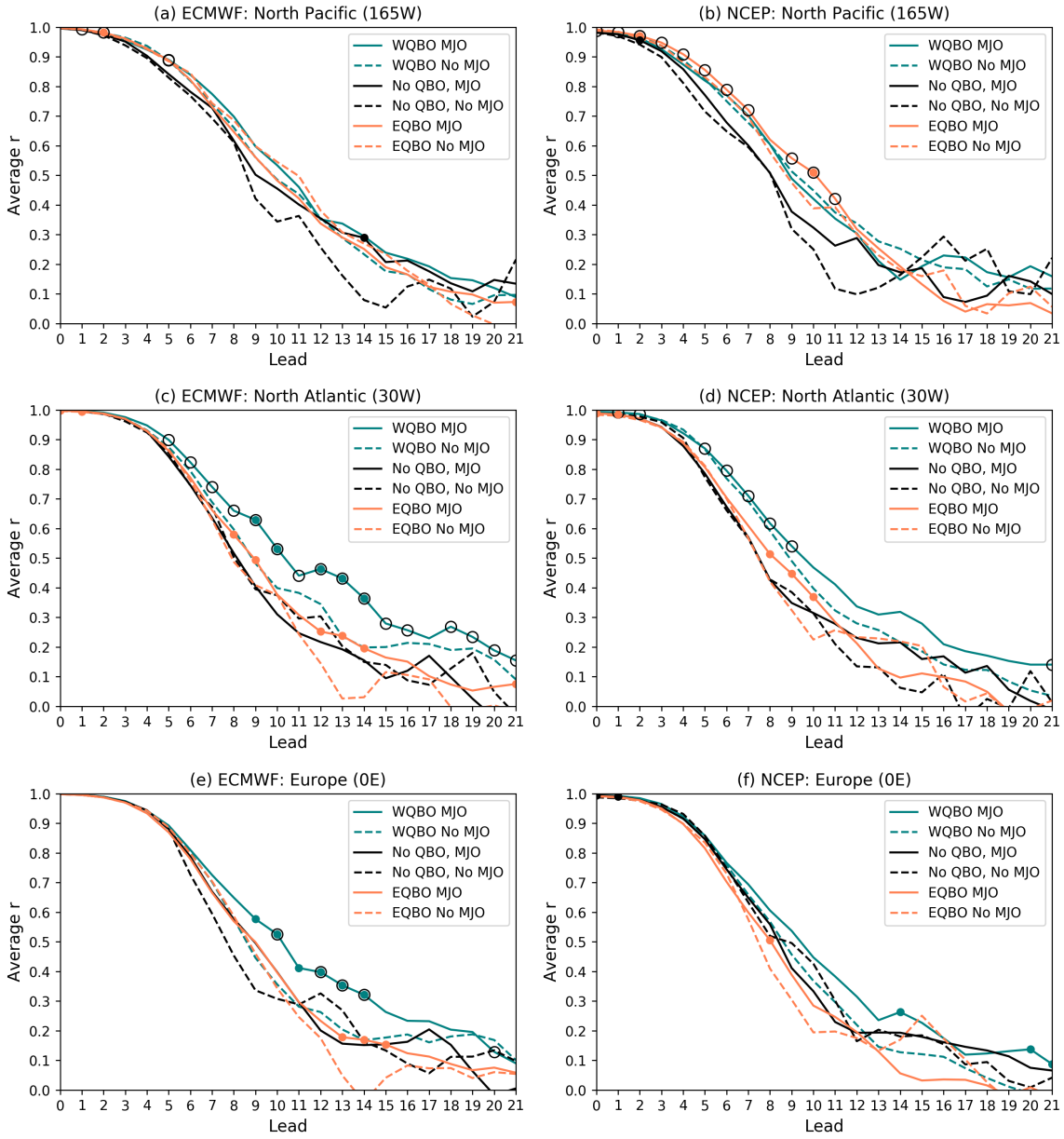

FIG. 4.1. Anomalous spatial correlation coefficient at (top) 150°W, (middle) 85°W and (bottom) 40°W for (left) ECMWF and (right) NCEP. Solid lines correspond to active MJOs while dashed lines correspond to inactive MJOs. Colors refer to the phase of the QBO. Colored dots denote significantly increased skill between active and inactive MJO under a specific QBO state at 95% confidence. Hollow black circles indicate a significantly increased skill between E/WQBO-MJO events and NQBO-MJO events at 95% confidence.

4.2 NORTHERN HEMISPHERE PREDICTION SKILL: DEPENDENCE ON ACTIVE MJO

While Figure 4.1 shows results for three specific regions, we extend these results to all longitudes in Figures 4.2 and 4.3. To determine how the impact of the MJO on midlatitude prediction skill changes

following a particular phase of the QBO (colored dots in Figure 4.1), we examine the difference between prediction skill following active MJOs compared to inactive MJOs during both EQBO and WQBO (Figure 4.2). Specifically, the four panels show the difference in ACC between EQBO-MJO and EQBO-noMJO (Figure 4.2a,b; orange solid and dashed lines in Figure 4.1) and WQBO-MJO and WQBO-noMJO (Figure 4.2c,d; teal solid and dashed lines in Figure 4.1). The left column of Figure 4.2 shows the differences within ECMWF and the right column shows differences within NCEP. Shading specifies increased prediction skill following the MJO compared to inactive MJOs during the specific phase of the QBO. Regions of significantly increased prediction skill following the MJO compared to inactive MJOs during the specific phase of the QBO are denoted with grey dots (orange and teal dots in Figure 4.1).

During EQBO in both models (Figure 4.2a,b), the Pacific exhibits increased prediction skill during active MJO events compared to inactive MJOs at Week 1 leads. There is also enhanced prediction skill following active MJOs starting in North America and extending to Europe (90-30°W) at Week 2-3 leads for ECMWF and through Week 2 for NCEP. In ECMWF, there appears to be an eastward propagation of enhanced prediction skill during EQBO from North America to the West Pacific starting around 12 days lead. In NCEP, we do not see this propagation of increased skill. This could be due to the lack of additional skill provided by the MJO following week 2 in NCEP that continues through Week 3 in ECMWF.

During WQBO in both models (Figure 4.2c,d), there is increased prediction skill following the MJO in the East Pacific into North America through Week 1. In ECMWF, this increased skill continues through Week 2 into the North Atlantic, but has no additional skill by Week 3 (Figure 4.2c). In NCEP, this additional prediction skill disappears during Week 2, but then reemerges in the East Pacific and over North America by Week 3 (Figure 4.2d).

From Figure 4.2 we see that in both models, active MJOs during EQBO generally lead to enhanced skill from the North Pacific to North America over Weeks 2-3 while active MJOs during WQBO generally lead to enhanced skill from the North Pacific through the North Atlantic over Weeks 1-2. The regions of enhanced prediction skill following active MJOs during EQBO and WQBO are not associated with enhanced prediction skill following active MJOs during NQBO (see Appendex Figure A6). This suggests that following MJO activity, subseasonal prediction skill is enhanced in the Pacific to the Atlantic by the MJO during strong QBOs while MJO activity during NQBO does not significantly enhance prediction skill.

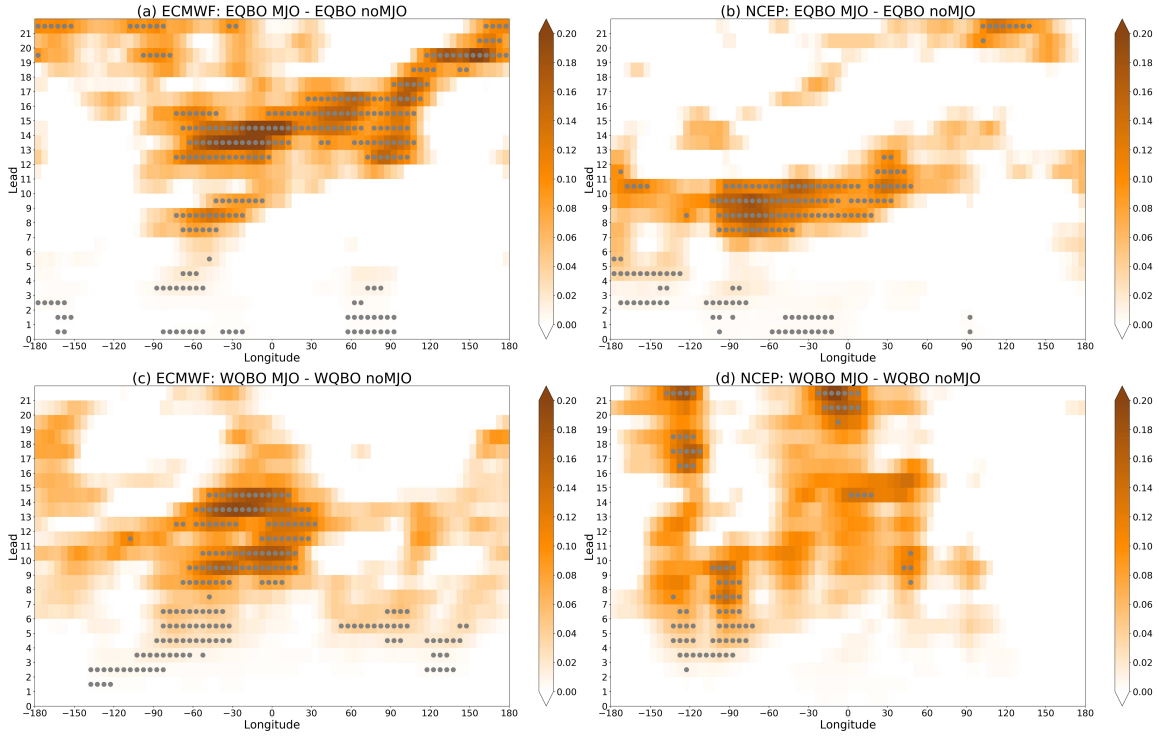

FIG. 4.2. Anomalous correlation coefficient between (top) EQBO-MJO and EQBO-noMJO and (bottom) WQBO-MJO and WQBO-noMJO for (left) ECMWF and (right) NCEP at each longitude and lead from model initialization. Correlations are calculated within a 60°wide box, centered on each longitude, extending from 30-60°N. Gray dots denote significant increases in prediction skill at 95% confidence from active MJO compared to inactive MJO under the specific QBO phase for the plot.

4.3 NORTHERN HEMISPHERE PREDICTION SKILL: DEPENDENCE ON ACTIVE QBO

To further explore the importance of QBO-MJO activity on subseasonal prediction, we examine the difference between prediction skill following active MJOs during E/WQBO compared to active MJOs during NQBO. Similar to Figure 4.2, the left column of Figure 4.3 shows the differences for ECMWF and the right column for NCEP. Specifically, the four panels show the difference in ACC between EQBO-MJO and NQBO-MJO (Figure 4.3a,b; orange and black solid lines in Figure 4.1) and WQBO-MJO and NQBO-MJO (Figure 4.3c,d; teal and black solid lines in Figure 4.1). As in Figure 4.1, black hollow circles indicate significant changes in prediction skill between the specified QBO and NQBO during active MJO.

During EQBO in both models (Figure 4.3a,b), there is mainly enhanced prediction skill following active MJOs over the Pacific in Week 1 compared to NQBO. This increased prediction skill over the Pacific continues through Week 2 in NCEP. For WQBO in both models (Figure 4.3c,d), there is also enhanced prediction skill following active MJOs compared to NQBO from Week 1 to 3 over the Pacific and

Atlantic. Specifically, this enhanced prediction skill in ECMWF (Figure 4.3c) is located in the Pacific and extends into the Atlantic for Weeks 1-2, and continues through the Atlantic during Week 3. In NCEP (Figure 4.3d), this enhanced prediction skill spans from the Pacific through the Atlantic during Week 1-3.

Note that in all panels, much of the enhanced skill is confined to a specific longitudinal region. Since the QBO oscillates with a period of about 28 months, we may expect enhanced prediction skill to remain around the same region through Week 3 when examining skill differences between QBO phases. However, this confined skill could also be due to a stationary rossby wave signal following strong QBO-MJOs that is not present following NQBO-MJOs. Therefore, since the prediction skill is enhanced and confined to a specific longitudinal region out to Week 3, we speculate that this enhanced non-propagating skill is likely from either a stationary rossby wave signal or enhanced skill from the strong QBOs effect on the midlatitudes compared to NQBO.

Since EQBO is thought to increase the amplitude of the MJO as well as help to propagate the MJO further into the Pacific Ocean compared to WQBO (Son et al. 2017; Nishimoto and Yoden 2017; Zhang and Zhang 2018), it may be expected that active MJOs during EQBO conditions will lead to stronger MJO teleconnections and thus, act to enhance subseasonal prediction in the midlatitudes. However, from Figure 4.3 we see that both EQBO *and* WQBO tend to have greater prediction skill compared to NQBO during active MJO across a range of longitudes and lead times. While unexpected, this result is partially supported by previous research, where enhanced prediction skill of Atmospheric Rivers over Alaska is found following active MJOs during WQBO (Baggett et al. 2017).

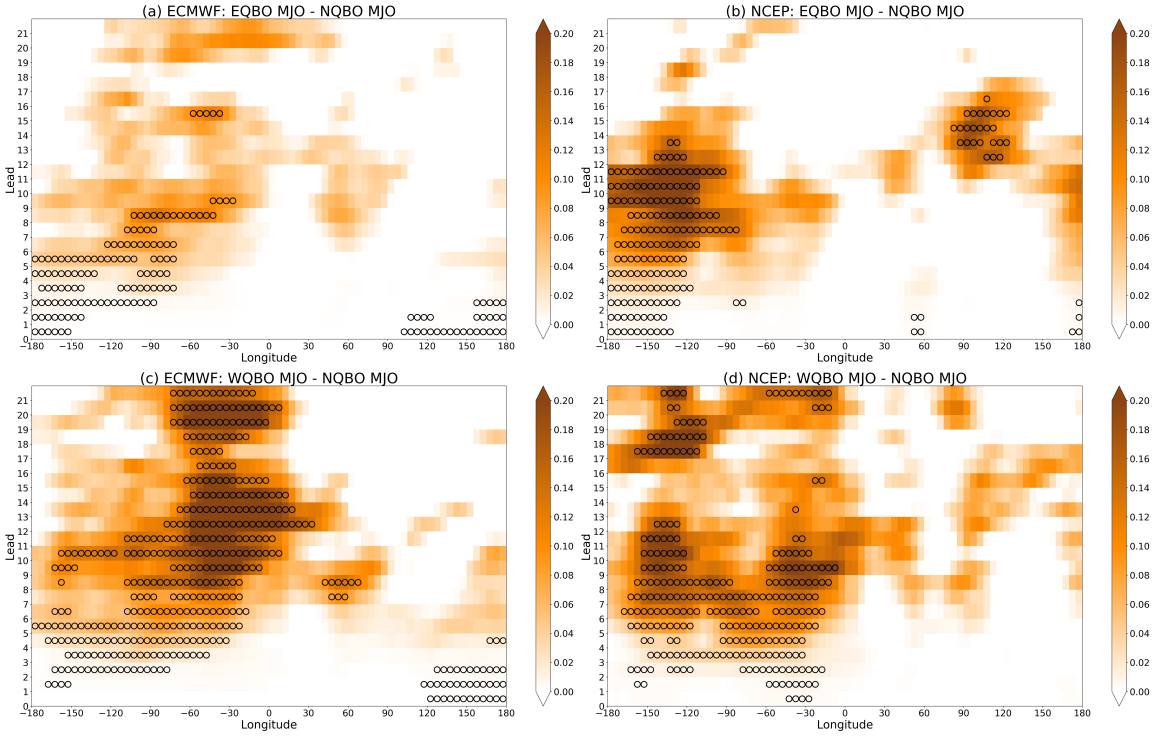

FIG. 4.3. Anomalous correlation coefficient between (top) EQBO-MJO and NQBO-MJO and (bottom) WQBO-MJO and NQBO-MJO for (left) ECMWF and (right) NCEP at each longitude and lead from model initialization. Correlations are calculated within a 60°wide box, centered on each longitude, extending from 30-60°N. Hollow black circles indicate significant increases in prediction skill at 95% confidence from E/WQBO-MJO activity compared to NQBO-MJO activity.

4.4 SUMMARY OF NORTHERN HEMISPHERE PREDICTION SKILL

The presence of both of these forms of significance (grey dots within hollow circles) represents where strong QBOs increase the impact of the MJO on midlatitude prediction skill. As a reminder, hollow circles indicate where there is significantly greater skill following E/WQBO-MJO than NQBO-MJO, while grey dots indicates where E/W/NQBO-MJO leads to significantly greater skill than E/W/NQBO-noMJO. To better visualize this overlap, Figure 4.4 combines both forms of significance from Figures 4.2 and 4.3 for ease of visualization, where grey dots are now orange (teal) for EQBO (WQBO). In EQBO in both models (Figure 4.4a,b), there is very little overlap of the two forms of significance (orange dots in hollow circles). On the other hand, for WQBO in both models (Figure 4.4c,d), most of the East Pacific and Atlantic that exhibit significantly increased prediction skill following active MJOs compared to inactive MJOs (teal dots) are collocated enhanced prediction skill following WQBO-MJO compared to NQBO-MJO (hollow circles). This indicates that there is significantly greater prediction skill following active MJOs compared to inactive MJOs during WQBO as well as active MJOs during NQBO. In other

words, WQBOs increase the impact of the MJO on midlatitude prediction skill between the East Pacific and Atlantic compared to NQBO.

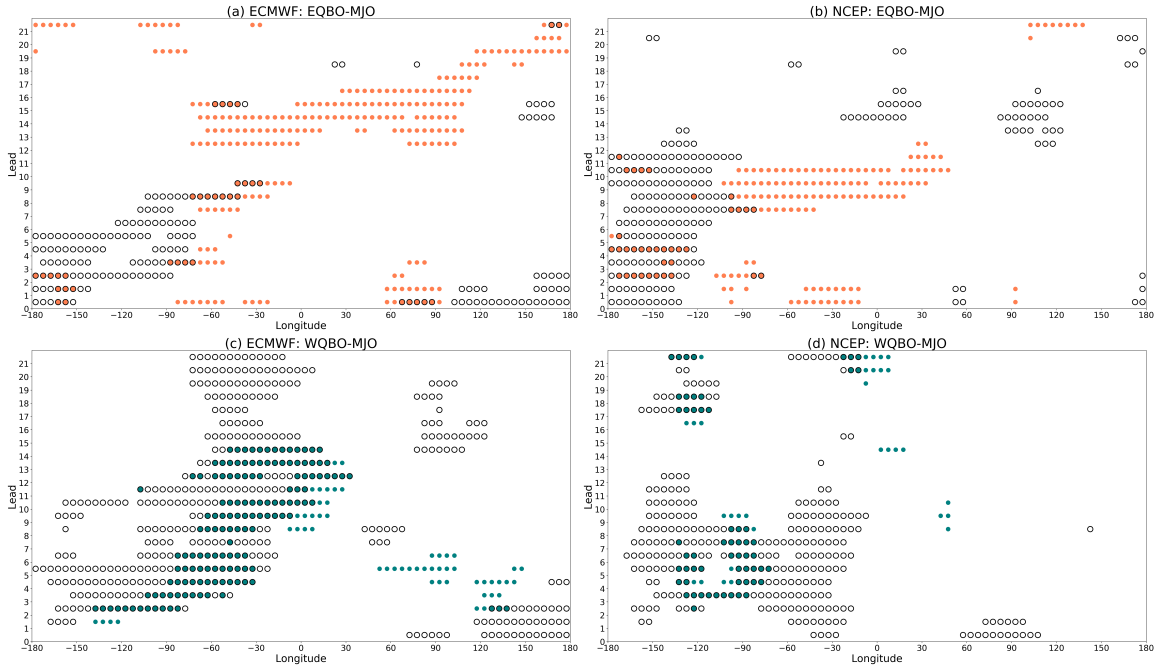

FIG. 4.4. Lead vs longitude plots with combined significance from Figure 4.2 and 4.3. Colored dots denote significant increases in prediction skill at 95% confidence from active MJO compared to inactive MJO under the specific QBO phase for the plot, where the color refers to the phase of the QBO. Orange is EQBO and teal is WQBO. Hollow black circles indicate significant increases in prediction skill at 95% confidence from E/WQBO-MJO activity compared to NQBO-MJO activity.

CHAPTER 5

RESULTS: PREDICTION SKILL AND NORTHERN HEMISPHERE SENSITIVITY

In Chapter 3, we saw that ECMWF and NCEP hindcasts generally capture regional sensitivity to the MJO under different phases of the QBO. From previous research, we also know that robust midlatitude circulation following certain phases of the MJO tends to have additional forecast skill (Tseng et al. 2018), and therefore, we may expect a link between regional sensitivities and increased prediction skill.

In an attempt to systematically examine the relationship between MJO sensitivity and prediction skill across all longitudes, STRIPES values are averaged from 30-60°N and compared to prediction skill averaged along leads 8-18 days (Figure 5.1). Days 8-18 are chosen based on previous research on MJO teleconnection timescales (e.g. Cassou 2008; Henderson et al. 2016; Tseng et al. 2019), however, these results are insensitive to variations of +/- 5 days. Figure 5.1 shows the average prediction skill across leads 8-18 days for EQBO in orange (Figure 5.1a,b) and WQBO in teal (Figure 5.1c,d) along with average STRIPES values in black for all longitudes. While one can certainly find locations where they appear to oscillate together, their correlations are low (see panel titles). The exception being NCEP during EQBO (Figure 5.1b) and ECMWF during WQBO (Figure 5.1c), where the correlation is around 0.5. For the other two panels, it appears that increased regional z500 sensitivity to the MJO in the Northern Hemisphere does not clearly translate to increased prediction skill. It is possible that these correlations are low due to differences in the signal-to-noise ratio between composites and daily spatial correlations.

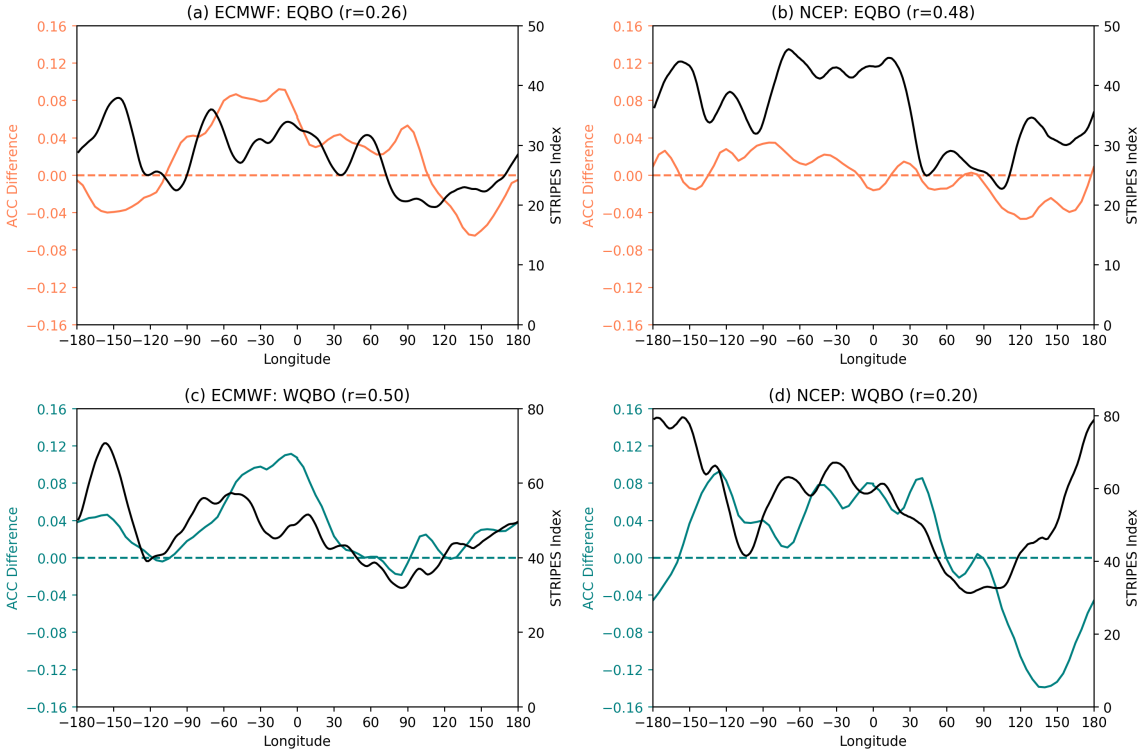

FIG. 5.1. Average change in prediction skill between active and inactive MJOs (color) across leads of 8-18 days and average STRIPES value (black) from 30°to 60°N for all longitudes. Colors refer to the phase of the QBO, where orange is EQBO and teal is WQBO. The correlation coefficient (r) is given in the title.

CHAPTER 6

CONCLUSIONS

The MJO is the dominant mode of intraseasonal variability in the tropics (Madden and Julian 1971; Adames and Kim 2016), and through its convective heating, modulates midlatitude weather, days to weeks after an MJO event (e.g. Vecchi 2004; Zhou et al. 2012; Henderson et al. 2016; Tseng et al. 2019). Recent research has shown that the QBO impacts MJO amplitude, propagation, and prediction skill (Son et al. 2017; Nishimoto and Yoden 2017; Zhang and Zhang 2018; Marshall et al. 2017; Lim et al. 2019) as well as modulates MJO teleconnections (e.g. Baggett et al. 2017; Mundhenk et al. 2018; Wang et al. 2018). This raises the question as to whether the QBO also affects the prediction skill of MJO teleconnections. The goal of this study is to address this question through an examination of differences in Week 1-3 prediction skill between different combinations of QBO-MJO activity.

Through a STRIPES analysis, we show that ECMWF and NCEP hindcasts are capable of simulating midlatitude MJO sensitivity, in a composite sense, out to Week 3 under different phases of the QBO. Thus, we use these hindcasts to study enhanced S2S prediction skill following QBO-MJO activity. Increased prediction skill is determined from significant increases in spatial correlations of z500 for various QBO-MJO combinations. First, comparing strong QBOs to NQBOs, we find that there is enhanced prediction skill following MJOs during EQBO over the Pacific, and enhanced prediction skill from the Pacific to Europe following MJOs during WQBO. Second, comparing active MJOs to inactive MJOs during different QBO phases, we find that when active MJOs occur during EQBOs, there is enhanced prediction skill in the Americas into Europe over Weeks 1-2 in both models and into the Pacific over Week 3 in ECMWF. During WQBO, this enhanced prediction skill is located in the Pacific through the Atlantic over Weeks 1-2. In contrast, there is no enhanced prediction skill following MJO activity compared to inactive MJOs during NQBO in these regions and suggests that the impact of the MJO on Northern Hemisphere prediction skill is only apparent during strong QBOs.

Together, these two forms of significance inform us on when and where strong QBOs increase the impact of the MJO on midlatitude prediction skill. Over North America (NCEP and ECMWF) and the Atlantic and Europe (ECMWF) following active MJOs, the two forms of significance overlap and thus, implies that WQBOs (compared to NQBO) increases the impact of the MJO on midlatitude prediction skill. On the other hand, regions with both forms of significance during EQBO are scarce. When

comparing all regions of enhanced prediction skill to regional sensitivity (STRIPES), we found no clear relationship, except possibly in ECMWF during WQBO and NCEP during EQBO.

This study provides insight on improved prediction skill following different MJO-QBO combinations; however, more research is needed to determine the causal link between the MJO-QBO, midlatitude teleconnections and prediction skill. It is unclear whether enhanced midlatitude prediction skill is a consequence of the QBO's direct effects on the tropical environment in which the MJO forms and/or through the modulation of the atmospheric basic state through which Rossby waves propagate.

In the beginning of this thesis, we attempt to motivate that enhanced MJO prediction following EQBO (Marshall et al. 2017; Lim et al. 2019) may also lead to enhanced midlatitude prediction skill following EQBO. However, Kim et al. (2020) (in Review) find no significant QBO-MJO prediction skill relationship within the SubX database. This may partially explain why we find both EQBO and WQBO lead to enhanced midlatitude prediction skill in these hindcasts rather than only EQBO, as the models do not significantly capture the QBO-MJO relationship. In terms of mechanisms, EQBO and WQBO may lead to enhanced prediction skill because following EQBO (WQBO) events, the polar vortex is known to weaken (strengthen) via the Holton-Tan effect (Holton and Tan 1980). Tripathi et al. (2015) showed that subseasonal hindcasts are able to successfully capture circulation anomalies following weak and strong polar vortex states. In addition, it has been shown that these polar vortex states lead to enhanced prediction skill in the Northern Hemisphere (e.g. Thompson and Wallace 1998; Baldwin et al. 2001). This may partially explain why there is enhanced prediction skill following active MJOs in *both* EQBO and WQBO; however, further research into the mechanisms is necessary. It should also be noted that while strong ENSO events were removed from our analysis, some influences from ENSO may remain. In addition, the sample sizes for MJO-QBO activity are small (Table A1). While we attempt to account for this through our statistical analysis, these results may change in time as more events occur. Even so, this work suggests that we need to reconsider the importance of WQBO on the MJO as well as further research the implications of the QBO on midlatitude S2S prediction skill.

CHAPTER 7

FUTURE WORK

Future work is required to round out the answer to whether the QBO also affects the prediction skill of MJO teleconnections. To do this, the analysis here should be applied to all models within the S2S database to obtain a broader understanding of hindcast prediction skill on S2S timescales. In addition, the control runs are utilized in this study in order to compare between models; however, using the ensemble mean for the analysis instead may increase the prediction skill of individual models and would allow for an examination of the utility of hindcast models on S2S timescales.

Since this work suggests that there is an impact of the QBO on midlatitude prediction skill, future work should next address *how* the QBO impacts it. The beginning of this thesis suggests that stronger and slower propagating MJOs (Son et al. 2017; Nishimoto and Yoden 2017; Densmore et al. 2019; Zhang and Zhang 2018) as well as enhanced MJO predictability (Marshall et al. 2017; Lim et al. 2019) during EQBO may lead to enhanced prediction skill of MJO teleconnections under EQBO. However, our results suggest that the easterly *and* westerly phase of the QBO are important for MJO teleconnection prediction skill on S2S timescales. A direct mechanism contributing to this enhanced skill is suggested in Chapter 6 but not examined. Therefore, possible mechanisms should be the focus of next steps.

A method for understanding the impacts of the QBO on extratropical circulation, and thus, MJO teleconnections, is through a linear baroclinic model, as in Tseng et al. (2020) (in Review). Through modifying the forcing and basic state of the model, the importance of QBO modulation of the MJO and/or modification of the basic state on MJO teleconnections can be examined. The importance of these mechanisms for prediction can also be calculated through a comparison between a high-top and low-top model (e.g. the CESM2 hindcast model), as in Kim et al. (2020) (in Review). In this way, the impact of the stratospheric resolution on the MJO and MJO teleconnections can be isolated through differences between model runs.

Following, a more detailed analysis of the ECMWF and NCEP hindcasts can be conducted based on the results from the linear baroclinic model and the high-top versus low-top experiment. For example, if the QBO's direct impact on the MJO (e.g. changes to upper tropospheric stability (Collimore et al. 2003; Garfinkel and Hartmann 2011a; Son et al. 2017)) is of importance for MJO teleconnections, the QBOs direct impact on the MJO within the S2S database should be studied. If however, the QBO's modification of the basic state appears to be important (e.g. impacts on the polar vortex and tropospheric

subtropical jet Simpson et al. 2009; Garfinkel and Hartmann 2011b; Holton and Tan 1980; Garfinkel et al. 2018)), an examination of the QBOs impact on extratropical circulation in the models should be conducted.

REFERENCES

Abhik, S. and H. H. Hendon, 2019: Influence of the QBO on the MJO during coupled model multiweek forecasts. *Geophys. Res. Lett.*

Adames, Á. F. and D. Kim, 2016: The MJO as a dispersive, convectively coupled moisture wave: Theory and observations. *J. Atmos. Sci.*, **73 (3)**, 913–941.

Baggett, C. F., E. A. Barnes, E. D. Maloney, and B. D. Mundhenk, 2017: Advancing atmospheric river forecasts into subseasonal-to-seasonal time scales. *Geophys. Res. Lett.*, **44 (14)**, 2017GL074 434.

Baldwin, M. P., L. J. Gray, T. J. Dunkerton, and others, 2001: The quasi-biennial oscillation. *Reviews of Geophysics*, **39 (2)**, 179–229.

Cassou, C., 2008: Intraseasonal interaction between the Madden-Julian oscillation and the north atlantic oscillation. *Nature*, **455 (7212)**, 523–527.

Collimore, C. C., D. W. Martin, M. H. Hitchman, A. Huesmann, and D. E. Waliser, 2003: On the relationship between the QBO and tropical deep convection. *J. Clim.*, **16 (15)**, 2552–2568.

Dee, D. P., et al., 2011: The ERA-Interim reanalysis: Configuration and performance of the data assimilation system. *Quart. J. Roy. Meteor. Soc.*, **137 (656)**, 553–597.

Densmore, C. R., E. R. Sanabia, and B. S. Barrett, 2019: QBO influence on MJO amplitude over the maritime continent: Physical mechanisms and seasonality. *Mon. Weather Rev.*, **147 (1)**, 389–406.

Garfinkel, C. I. and D. L. Hartmann, 2011a: The influence of the Quasi-Biennial oscillation on the troposphere in winter in a hierarchy of models. part i: Simplified dry GCMs. *J. Atmos. Sci.*, **68 (6)**, 1273–1289.

Garfinkel, C. I. and D. L. Hartmann, 2011b: The influence of the Quasi-Biennial oscillation on the troposphere in winter in a hierarchy of models. part II: Perpetual winter WACCM runs. *J. Atmos. Sci.*, **68 (9)**, 2026–2041.

Garfinkel, C. I., C. Schwartz, D. I. V. Domeisen, S.-W. Son, A. H. Butler, and I. P. White, 2018: Extratropical atmospheric predictability from the Quasi-Biennial oscillation in subseasonal forecast models. *J. Geophys. Res. D: Atmos.*, **140**, 1.

Henderson, S. A., E. D. Maloney, and E. A. Barnes, 2016: The influence of the Madden–Julian oscillation on northern hemisphere winter blocking. *J. Clim.*, **29 (12)**, 4597–4616.

Holton, J. R. and H.-C. Tan, 1980: The influence of the equatorial Quasi-Biennial oscillation on the global circulation at 50 mb. *J. Atmos. Sci.*, **37 (10)**, 2200–2208.

Hoskins, B. J. and D. J. Karoly, 1981: The steady linear response of a spherical atmosphere to thermal and orographic forcing. *J. Atmos. Sci.*, **38 (6)**, 1179–1196.

Jenney, A. M., D. A. Randall, and E. A. Barnes, 2019: Quantifying regional sensitivities to periodic events: Application to the MJO. *J. Geophys. Res. D: Atmos.*, **124 (7)**, 3671–3683.

Kim, H., J. H. Richter, and Z. Martin, 2020: Insignificant qbo-mjo prediction skill relationship in the subseasonal reforecasts.

Lim, Y., S.-W. Son, A. G. Marshall, H. H. Hendon, and K.-H. Seo, 2019: Influence of the QBO on MJO prediction skill in the subseasonal-to-seasonal prediction models. *Clim. Dyn.*, **53 (3)**, 1681–1695.

Madden, R. A., 1986: Seasonal variations of the 40-50 day oscillation in the tropics. *J. Atmos. Sci.*, **43 (24)**, 3138–3158.

Madden, R. A. and P. R. Julian, 1971: Detection of a 40–50 day oscillation in the zonal wind in the tropical pacific. *J. Atmos. Sci.*, **28 (5)**, 702–708.

Madden, R. A. and P. R. Julian, 1972: Description of Global-Scale circulation cells in the tropics with a 40–50 day period. *J. Atmos. Sci.*, **29 (6)**, 1109–1123.

Madden, R. A. and P. R. Julian, 1994: Observations of the 40–50-day tropical Oscillation—A review. *Mon. Weather Rev.*, **122 (5)**, 814–837.

Marshall, A. G., H. H. Hendon, S.-W. Son, and Y. Lim, 2017: Impact of the quasi-biennial oscillation on predictability of the Madden–Julian oscillation. *Clim. Dyn.*, **49 (4)**, 1365–1377.

Mori, M. and M. Watanabe, 2008: The growth and triggering mechanisms of the PNA: A MJO-PNA coherence. *Journal of the Meteorological Society of Japan*, **86 (1)**, 213–236.

Mundhenk, B. D., E. A. Barnes, E. D. Maloney, and C. F. Baggett, 2018: Skillful empirical subseasonal prediction of landfalling atmospheric river activity using the Madden–Julian oscillation and quasi-biennial oscillation. *npj Climate and Atmospheric Science*, **1 (1)**, 20 177.

Nishimoto, E. and S. Yoden, 2017: Influence of the stratospheric Quasi-Biennial oscillation on the Madden–Julian oscillation during austral summer. *J. Atmos. Sci.*, **74 (4)**, 1105–1125.

Sardeshmukh, P. D. and B. J. Hoskins, 1988: The generation of global rotational flow by steady idealized tropical divergence. *J. Atmos. Sci.*, **45 (7)**, 1228–1251.

Simpson, I. R., M. Blackburn, and J. D. Haigh, 2009: The role of eddies in driving the tropospheric response to stratospheric heating perturbations. *J. Atmos. Sci.*, **66 (5)**, 1347–1365.

Son, S.-W., Y. Lim, C. Yoo, H. H. Hendon, and J. Kim, 2017: Stratospheric control of the Madden–Julian oscillation. *J. Clim.*, **30 (6)**, 1909–1922.

Sun, L., H. Wang, and F. Liu, 2019: Combined effect of the QBO and ENSO on the MJO. *Atmospheric and Oceanic Science Letters*, **12 (3)**, 170–176.

Sun, S., R. Bleck, S. G. Benjamin, B. W. Green, and G. A. Grell, 2018: Subseasonal forecasting with an icosahedral, vertically Quasi-Lagrangian coupled model. part i: Model overview and evaluation of systematic errors. *Mon. Weather Rev.*, **146 (5)**, 1601–1617.

Thompson, D. W. J. and J. M. Wallace, 1998: The arctic oscillation signature in the wintertime geopotential height and temperature fields. *Geophys. Res. Lett.*, **25 (9)**, 1297–1300.

Tripathi, O. P., et al., 2015: The predictability of the extratropical stratosphere on monthly time-scales and its impact on the skill of tropospheric forecasts: Stratospheric predictability and tropospheric forecasts. *Q.J.R. Meteorol. Soc.*, **141 (689)**, 987–1003.

Tseng, K.-C., E. Barnes, and E. Maloney, 2020: The consistency of mjo teleconnection patterns on interannual timescales.

Tseng, K.-C., E. A. Barnes, and E. D. Maloney, 2018: Prediction of the midlatitude response to strong Madden-Julian oscillation events on S2S time scales: PREDICTION OF Z500 AT S2S TIME SCALES. *Geophys. Res. Lett.*, **45 (1)**, 463–470.

Tseng, K.-C., E. Maloney, and E. Barnes, 2019: The consistency of MJO teleconnection patterns: An explanation using linear rossby wave theory. *J. Clim.*, **32 (2)**, 531–548.

Vecchi, G. A., 2004: The Madden-Julian oscillation (MJO) and northern high latitude wintertime surface air temperatures. *Geophys. Res. Lett.*, **31 (4)**, 3500.

Vitart, F., 2017: Madden-Julian oscillation prediction and teleconnections in the S2S database: MJO prediction and teleconnections in the S2S database. *Q.J.R. Meteorol. Soc.*, **143 (706)**, 2210–2220.

Wang, J., H.-M. Kim, E. K. M. Chang, and S.-W. Son, 2018: Modulation of the MJO and north pacific storm track relationship by the QBO. *J. Geophys. Res. D: Atmos.*, **123 (8)**, 3976–3992.

Wheeler, M. C. and H. H. Hendon, 2004: An All-Season Real-Time multivariate MJO index: Development of an index for monitoring and prediction. *Mon. Weather Rev.*, **132 (8)**, 1917–1932.

Yoo, C. and S.-W. Son, 2016: Modulation of the boreal wintertime Madden-Julian oscillation by the stratospheric quasi-biennial oscillation. *Geophys. Res. Lett.*, **43 (3)**, 2016GL067 762.

Zhang, C. and B. Zhang, 2018: QBO-MJO connection. *J. Geophys. Res. D: Atmos.*, **123 (6)**, 2957–2967.

Zheng, C., E. Kar-Man Chang, H.-M. Kim, M. Zhang, and W. Wang, 2018: Impacts of the Madden–Julian oscillation on Storm-Track activity, surface air temperature, and precipitation over north america. 6113–6134 pp.

Zhou, S., M. L'Heureux, S. Weaver, and A. Kumar, 2012: A composite study of the MJO influence on the surface air temperature and precipitation over the continental united states. *Clim. Dyn.*, **38 (7)**, 1459–1471.

APPENDIX

SUPPLEMENTAL MATERIAL

ECMWF				NCEP			
without ENSO	N	with ENSO	N	without ENSO	N	with ENSO	N
MJO	326		870	MJO	233		724
no MJO	161		437	no MJO	127		356
EQBO-MJO	162		384	EQBO-MJO	112		340
WQBO-MJO	90		340	WQBO-MJO	65		256
NQBO-MJO	74		142	NQBO-MJO	56		128

TABLE A1. Sample sizes for combinations of QBO-MJO for ECMWF and NCEP with and without ENSO.

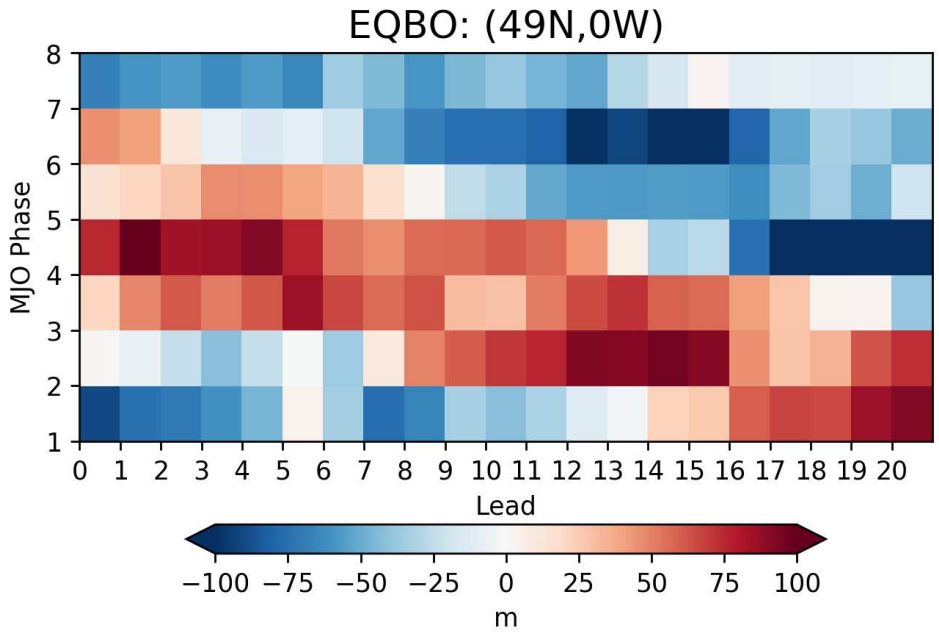

FIG. A1. Boreal winter (DJF) composite ERA-I z500 anomalies subsampled to ECMWF initialization dates (1995-2016) for each MJO phase during EQBO vs lead at 49N and 0W.

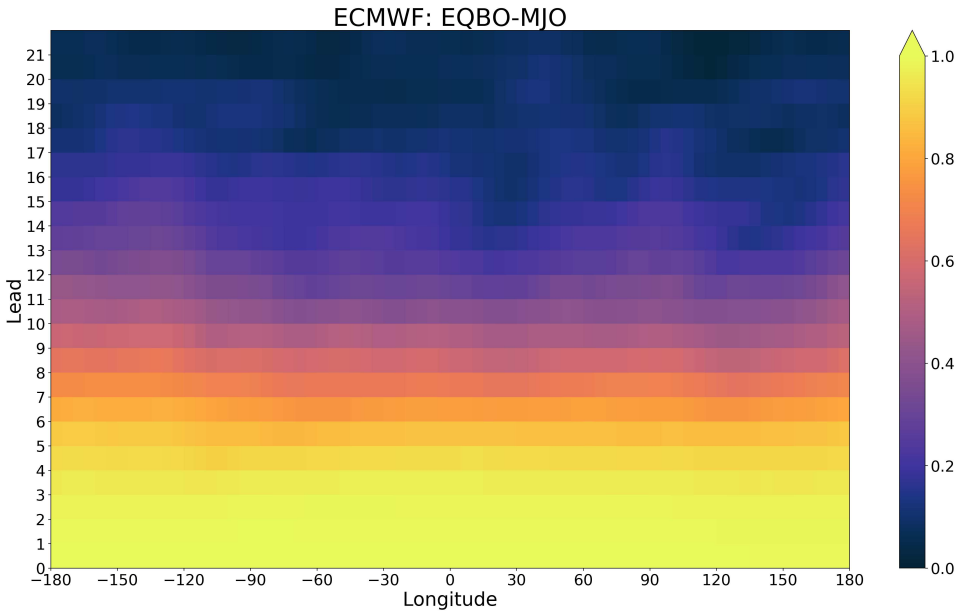

FIG. A2. Spatial correlations between ERA-I and ECMWF across longitudes and for leads 0-21 days averaged over EQBO-MJO events. Correlations are calculated within a 60°wide longitude box, centered at each longitude spanning 30-60°N.

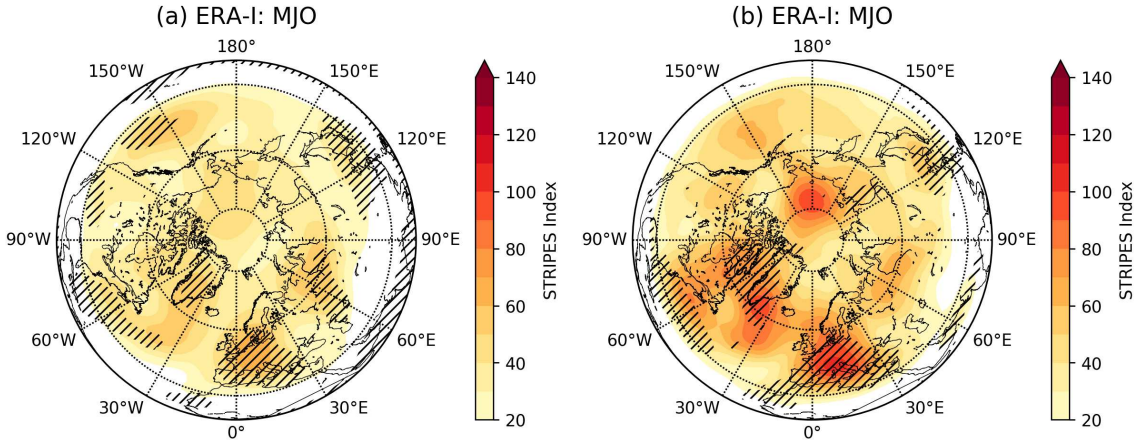

FIG. A3. STRIPES values for (a) ECMWF hindcasts' dates in ERA-I and (b) NCEP hindcasts' dates in ERA-I for all MJO events. Black hatches denote STRIPES values that are statistically larger than expected by chance at 90% confidence in ERA-I.

A1 NORTHERN HEMISPHERE NEGATIVE PREDICTION SKILL

This thesis focuses on the regions of enhanced prediction skill following active MJOs compared to inactive MJOs under a particular QBO phase *and* active MJO during strong QBOs compared to NQBO.

Enhanced prediction skill is examined because enhanced MJO and QBO activity may provide a prominent signal above model noise and uncertainty. For completeness, here we note the decrease in prediction skill following active MJOs compared to inactive MJOs during both EQBO and WQBO (Figure A4) as well as the decrease in prediction skill following active MJOs during strong QBOs compared to NQBO (Figure A5).

In Figure A4, the four panels show the difference in ACC between EQBO-MJO and EQBO-noMJO (Figure A4a,b) and WQBO-MJO and WQBO-noMJO (Figure A4c,d). The left column of Figure A4 shows the differences within ECMWF and the right column shows differences within NCEP. As in Figure 4.2, grey dots denote significance, but now only for regions with significantly decreased prediction skill following active MJOs. Through Week 1 and into Week 2, both ECMWF and NCEP (Figure A4a,b) have decreased skill following active MJOs during EQBO from Russia into the western Pacific. In addition, NCEP has decreased skill over the Atlantic during Week 2 and 3 following EQBO-MJOs, but this is not the case for ECMWF. For WQBO, there is also decreased skill following active MJOs in the central Pacific in Week 1 for both models (Figure A4c,d). This skill extends into the western Pacific on Week 2 timescales in NCEP (Figure A4d). In both models, decreased skill following WQBO-MJOs reappears at the end of Week 3 over the western Pacific.

Similar to Figure A4, Figure A5 has four panels which show the difference in ACC between EQBO-MJO and NQBO-MJO (Figure A5a,b) and WQBO-MJO and NQBO-MJO (Figure A5c,d). The left column of Figure A5 shows the differences for ECMWF and the right column for NCEP. As in Figure 4.3, black hollow circles indicate significance, but now only for regions with significantly decreased prediction skill following active MJOs under a specified QBO compared to under NQBO. In NCEP, there is decreased prediction skill following EQBO-MJO compared to NQBO-MJO at Week 3 from the eastern Atlantic through Europe. However, this decreased skill is not apparent in ECMWF. In addition, in ECMWF, there is decreased prediction skill following WQBO-MJO compared to NQBO-MJO at Week 3 over central Russia. However, this region does not have decreased prediction skill in NCEP. Therefore, there appears to be no regions consistent between the models where strong QBOs have decreased skill compared to active MJOs during NQBOs.

Overall, only a few regions have colocated decreased prediction skill following active MJOs compared to inactive MJOs during strong QBOs between the models. There are also no significant regions of decreased prediction skill colocated in ECMWF and NCEP hindcasts following active MJOs during strong QBOs compared to NQBO. Therefore, there are mainly regions of enhanced prediction skill (see

Chapter 4) and few-to-no regions of significantly decreased prediction skill following enhanced QBO and MJO activity, consistent with our signal-to-noise argument.

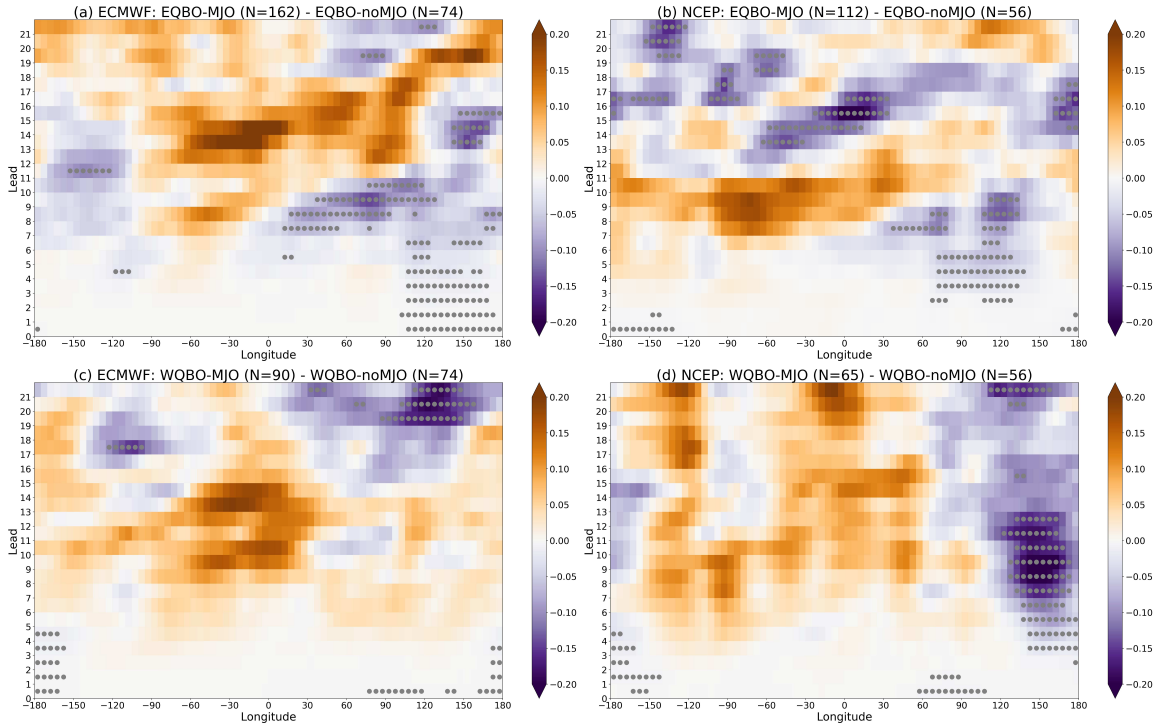

FIG. A4. Anomalous correlation coefficient between (top) EQBO-MJO and EQBO-noMJO and (bottom) WQBO-MJO and WQBO-noMJO for (left) ECMWF and (right) NCEP at each longitude and lead from model initialization. Gray dots denote significant decreases at 95% confidence in prediction skill from active MJO compared to inactive MJO under the specific QBO phase for the plot.

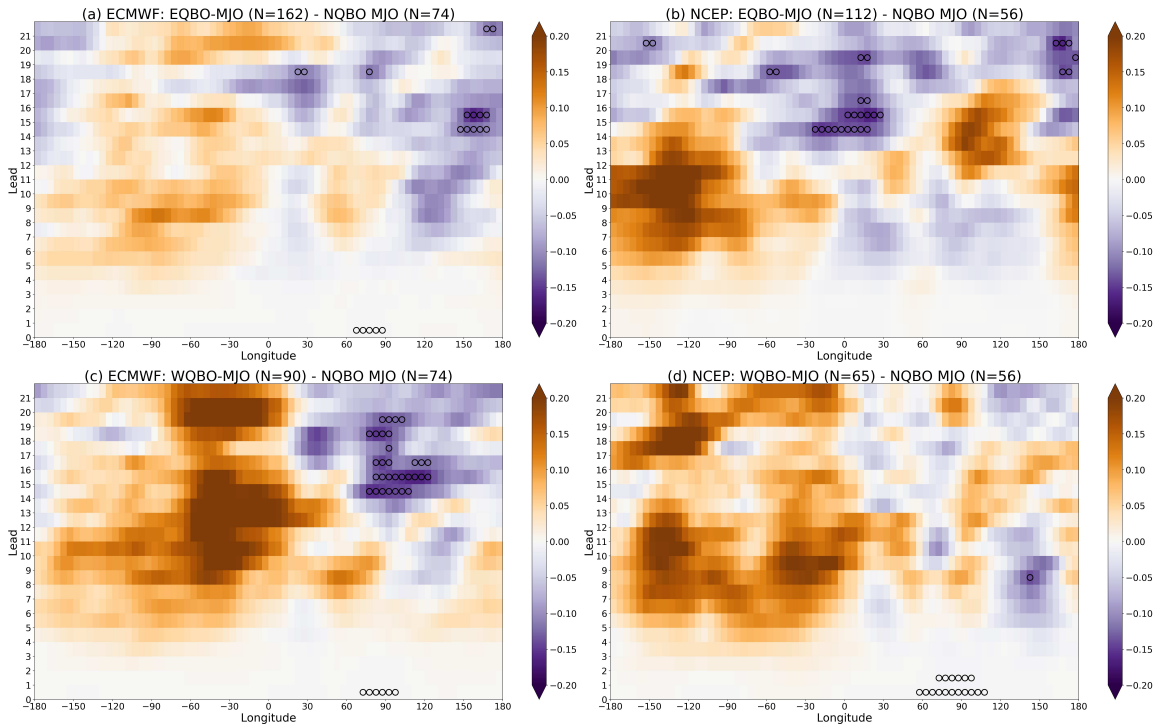

FIG. A5. Anomalous correlation coefficient between (top) EQBO-MJO and NQBO-MJO and (bottom) WQBO-MJO and NQBO-MJO for (left) ECMWF and (right) NCEP at each longitude and lead from model initialization. Hollow black circles indicate significant decreases at 95% confidence in prediction skill from E/WQBO-MJO activity compared to NQBO-MJO activity.

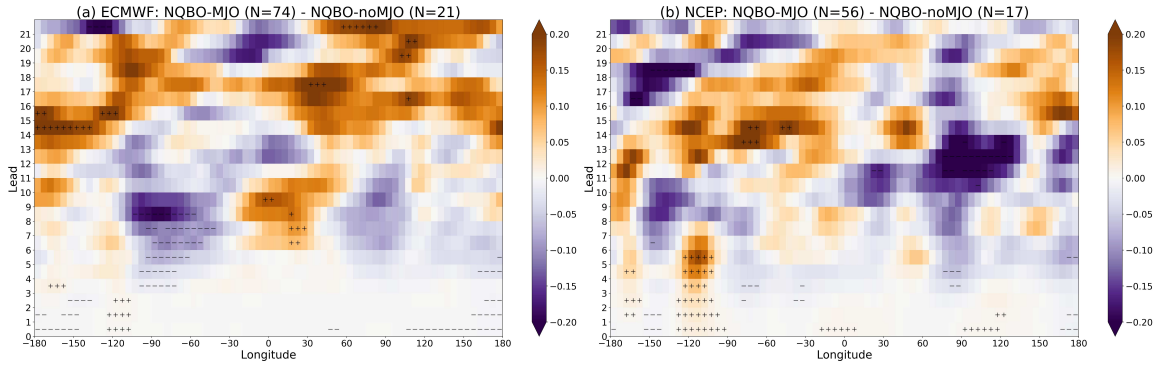

FIG. A6. Anomalous correlation coefficient between NQBO-MJO and NQBO-noMJO for (a) ECMWF and (b) NCEP at each longitude and lead from model initialization. The '+'/'-' denote significant increases/decreases at 95% confidence in prediction skill from active MJO compared to inactive MJO under NQBO.

A2 RESULTS INCLUDING ENSO

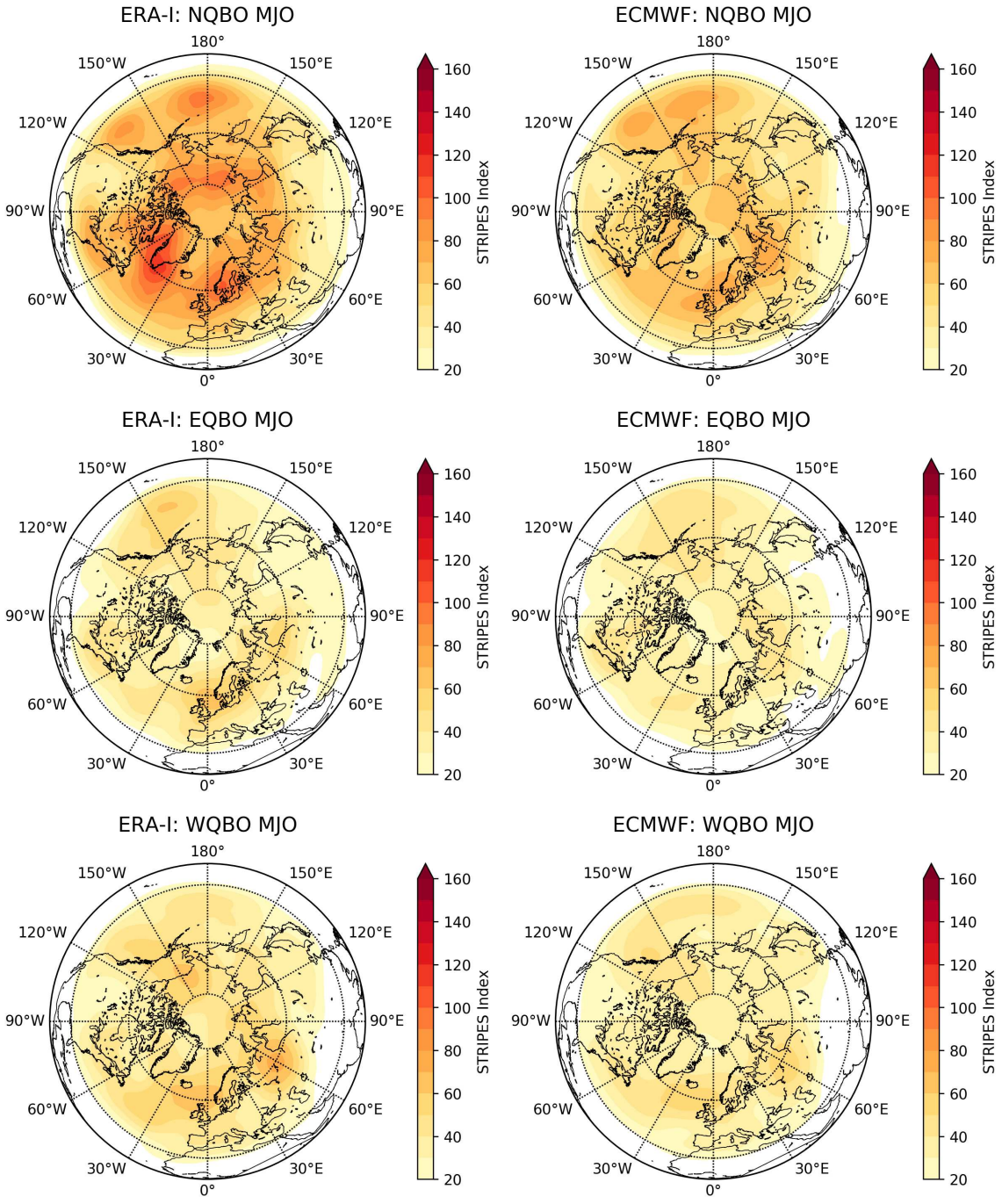

FIG. A7. STRIPES values for (left) ERA-Interim and (right) ECMWF for all (top) NQBO-MJO, (middle) EQBO-MJO and (bottom) WQBO-MJO events with ENSO.

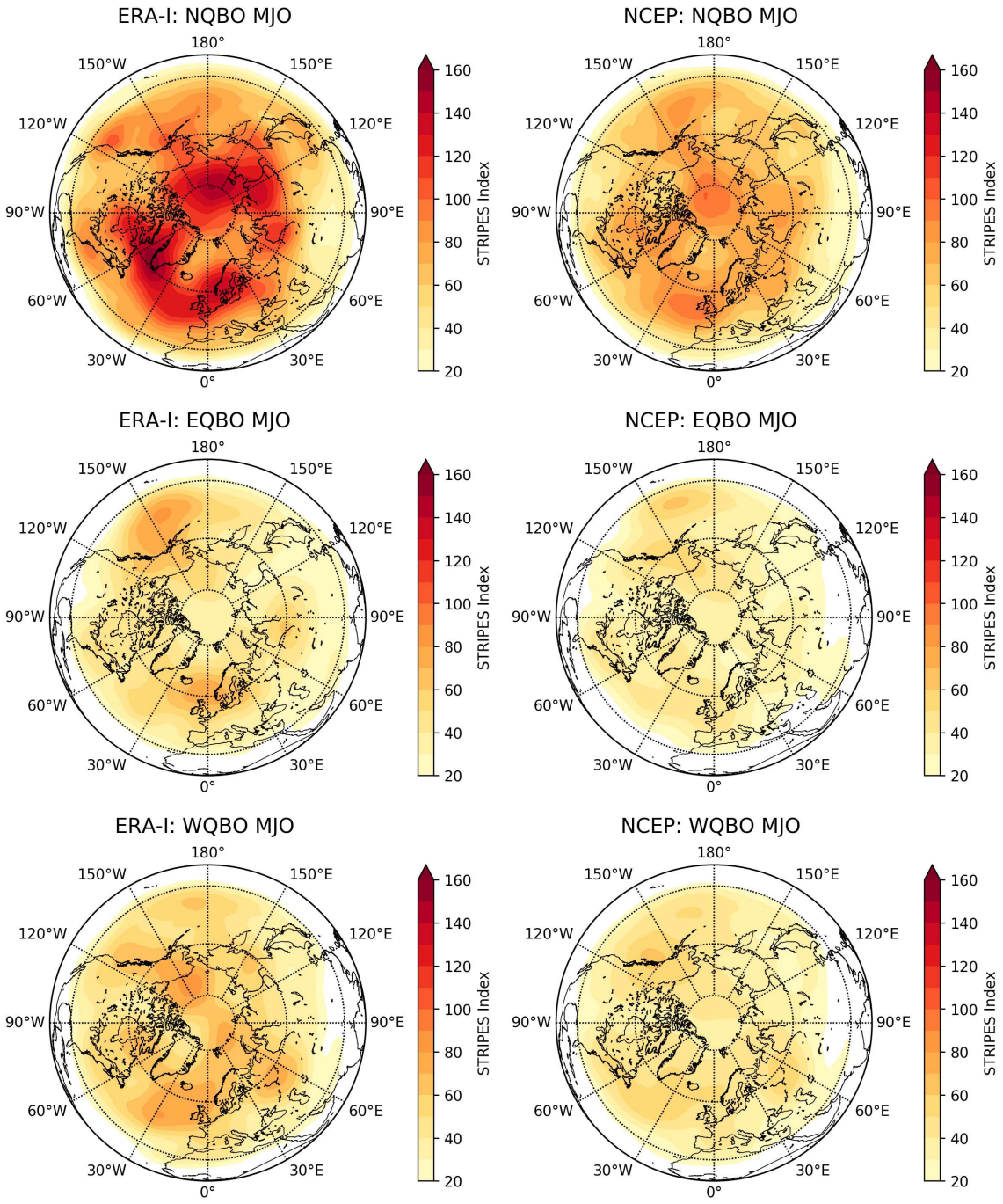

FIG. A8. STRIPES values for (left) ERA-Interim and (right) NCEP for all (top) NQBO-MJO, (middle) EQBO-MJO and (bottom) WQBO-MJO events with ENSO.

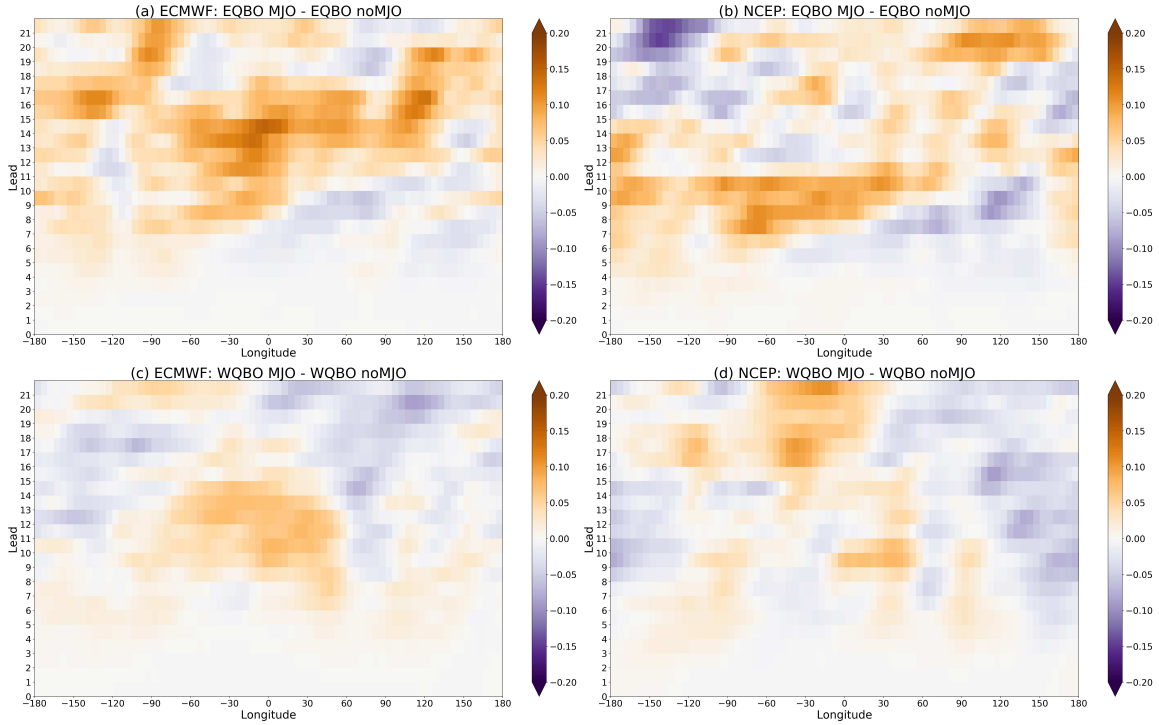

FIG. A9. Anomalous correlation coefficient with ENSO included between (top) EQBO-MJO and EQBO-noMJO and (bottom) WQBO-MJO and WQBO-noMJO for (left) ECMWF and (right) NCEP at each longitude and lead from model initialization.

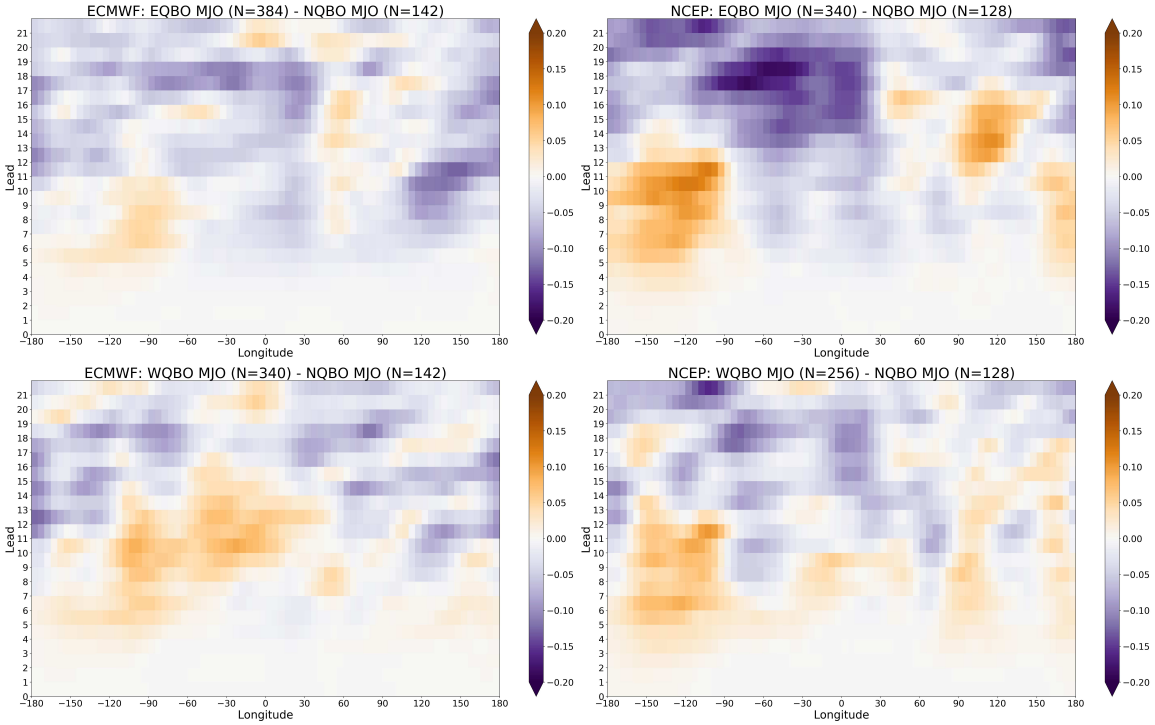

FIG. A10. Anomalous correlation coefficient with ENSO included between (top) EQBO-MJO and NQBO-MJO and (bottom) WQBO-MJO and NQBO-MJO for (left) ECMWF and (right) NCEP at each longitude and lead from model initialization.